Using TEM Diffraction to Analyze Crystal Structures

Luc Schnell

November 29, 2017

Abstract

Diffraction patterns generated in a transmission electron microscope (TEM) can be analyzed to determine the crystal structure of a sample material. For the specific case of the face-centered cubic (FCC) lattice materials silver and aluminum, it is shown how experimental diffraction patterns can be generated and compared to a theoretical pattern derived from first principles. The described methods can be easily adapted to other materials and lattice types.

1 Introduction

1.1 Transmission Electron Microscopy

Due to the small de Broglie wavelength $\lambda = \frac{h}{p}$ of electron matter waves (0.039 Å at an energy of 100 keV), transmission electron microscopy (TEM) can be used to probe structures on the scale of atom diameters. An electron beam incident on a crystalline material is reflected at the different lattice layers. Positive interference between the different reflected electron matter waves occurs, when the path length difference between them amounts to an integer multiple of the wavelength λ. Since the matter waves are monochromatic (the wavelength λ is given by the accelerating voltage of the electron gun), the path length difference is only a function of the angle under which the waves are reflected. Thus, we only expect to see positive interference under certain angles. By using a sample that contains many crystalline deposits oriented randomly in space, a ring diffraction pattern is generated. This pattern can then be analyzed using wave diffraction theory to determine the lattice type of the sample material (see next Section).

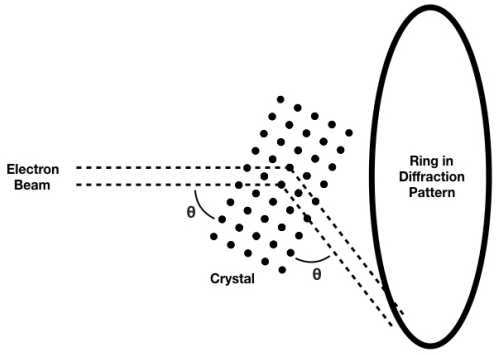

Figure 1: Diffraction in crystals

The challenges of transmission electron microscopy are that an electron beam needs to be produced, accelerated and focussed using high voltage and that a high vacuum needs to be achieved inside the microscope to minimize the effect of the air molecules on the path of the electron beam.

1.2 Diffraction in FCC Crystals

The theory of Fourier transformations is used to predict the diffraction patterns generated by crystal lattices in transmission electron microscopy. Here we will look at the specific case of a face-centered cubic (FCC) lattice, but the theory can be easily adapted to other lattice types.
It is assumed that the general diffraction condition $2\mathbf{k} \cdot \mathbf{G} = \mathbf{G}^2$, where $\mathbf{k}$ is the wave vector of the incoming wave and $\mathbf{G}$ a vector in the reciprocal crystal lattice is known to the reader. A detailed derivation of this formula from first principles is given in [2, p. 32]. The diffraction condition can be rewritten as

$$\frac{4\pi}{\lambda} \sin(\theta) = \|h\mathbf{b_1} + k\mathbf{b_2} + l\mathbf{b_3}\|, \tag{1}$$

where λ is the wavelength of the incident wave, 2θ is the angle between the incident and reflected wave, and $\mathbf{b_1}, \mathbf{b_2}, \mathbf{b_3}$ are the axis vectors of the reciprocal crystal lattice. The three integers h, k, l are the Miller indices of the crystal plane considered. Inserting the values for the primitive axes of the FCC lattice [2, p. 38], above formula becomes

$$2 \underbrace{\frac{a}{\sqrt{3(h^2+k^2+l^2) - 2(hk+kl+lh)}}}_{d_{hkl}} \sin(\theta) = n\lambda, \tag{2}$$

where a is the lattice parameter. Equation (2) is nothing else but the well-known Bragg formula, with the distance d_{hkl} between crystal planes denoted by the Miller indices h, k, l. Note that these indices are with respect to the primitive axes of the FCC lattice. We can rewrite (2) as

$$d_{hkl} = n\frac{\lambda}{2\sin(\theta)} \equiv n\left(\frac{K}{D}\right), \tag{3}$$

where $K = \frac{\lambda D}{2\sin(\theta)}$ is the so-called camera constant and D is the radius of the corresponding ring in the diffraction pattern. The expression for d_{hkl} in (2) can be used together with equation (3) to generate a theoretical diffraction pattern (see next Section).

2 Methods and Apparatus

2.1 Theoretical Diffraction Pattern

The distances d_{hkl} between crystal planes that produce a ring in the diffraction pattern can be found by inserting positive integer values $0, 1, 2, ...$ for the Miller indices h, k, l in (2). This was done in a Python script for $h, k, l \in \{0, 1, 2, ..., 10\}$. Since the expression for d_{hkl} in (2) is completely symmetric in h, k, l, we expect many of the d_{hkl} to have the same value (for example 100, 010 and 001 all yield the same value $d_{100} = d_{010} = d_{001}$). Since only the set of possible values $\{d_{hkl}\}$ is relevant for the further analysis, but not the multiplicities of these values, each value only needs to be stored once. The Python package OrderedSet provides an elegant way of solving this task. Assuming K to be constant in D, a theoretical diffraction pattern can be plotted based on (3), as soon as the layer distances d_{hkl} are known.

2.2 Electron Microscope

The transmission electron microscope HU-11A from Hitachi was used in this experiment. The high vacuum (10^{-1} to 10^{-4} Pa [4]) needed inside the TEM for electron diffraction was achieved using both mechanical and diffusion pumps. The TEM settings that were used to get a diffraction pattern are listed below.
An accelerating voltage for the electron beam of 95 kV was chosen for all measurements. At lower voltages, the wavelength λ of the electron matter waves would be longer and therefore considering (3) we would expect larger scattering angles θ, which would give a more distinct diffraction pattern. However, at lower voltages, more electrons are absorbed by the sample material (due to the decrease in energy), which results in the diffraction pattern having a lower brightness. The voltage 95 kV seems to be a good compromise between the size and the brightness of the diffraction rings.

Knob	Setting
Accelerating voltage	(95 ± 5) kV
Filament current	(25 ± 1) μA
Intermediate lens	adjust to get sharp and distinct pattern
Condenser lens 1	turned off
Condenser lens 2	(35 ± 1) mA
Projection lens	adjust to get sharp pattern
Object lens	(24 ± 1) mA

The intermediate lens and the projection lens need to be adjusted to get a sharp and distinct diffraction pattern. Different settings were chosen for the different sample materials. It should be noted that the radii of the rings in the diffraction pattern varied as the current (focal length) of these two lenses were changed. Considering (3) one can thus conclude that the camera constant K must be dependent on the lens settings. The diffraction patterns were made visible by a fluorescent screen placed inside the electron microscope. The pictures were taken using the camera Guppy from Allied Vision. It was calibrated to correct for the perspective-based distortion, since the camera obviously had to be placed outside the TEM, so that it doesn't get in the way of the electron beam.

2.3 Camera Constant

Comparing the diffraction patterns measured with the TEM to the theoretical diffraction pattern that was calculated in the Python script, the Miller indices of the different rings can be determined. Once this information is available, the camera constant K can be calculated via (3) as a function of the radius D (since d_{hkl} for each ring in the pattern is now known). The radii of the rings in the diffraction patterns were measured in pixels using a software called Traxis. This software, originally designed to analyze bubble chamber pictures in particle physics, is able to fit circles to points chosen in a picture. The pixel-to-centimeter conversion was found by measuring a known distance on the fluorescent screen in Traxis.

3 Results and Discussion

3.1 Theoretical Diffraction Pattern

The first eight layer distances d_{hkl} (the ones that were visible in the experiment) calculated in the Python script described in Section 2.1 are given in the table below.

Miller indices (conventional ax.)	Miller indices (primitive ax.)	d_{hkl} (in terms of the lattice param. a)
111	001	0.57735
002	011	0.50000
022	112	0.35355
113	012	0.30151
222	002	0.28868
004	022	0.25000
133	113	0.22942
024	123	0.22361

The Miller indices with respect to the conventional lattice axes are either all even or all odd. The same result can be found by calculating the structure factor of the FCC lattice interpreted as a simple cubic (SC) lattice with a two-atom basis, as done in [2, p. 41]. The formulas derived via the primitive cell in Section 1.2, however, are more general and easier to adapt to other lattice types. The lattice parameters a for the materials silver and aluminum are 4.09 Å and 4.05 Å respectively [2, p. 20], resulting in layer distances on the order of 1 Å. The resulting theoretical diffraction pattern is displayed in Figure 2. The Miller indices of the first eight diffraction rings were added to the plot in an image editing software.

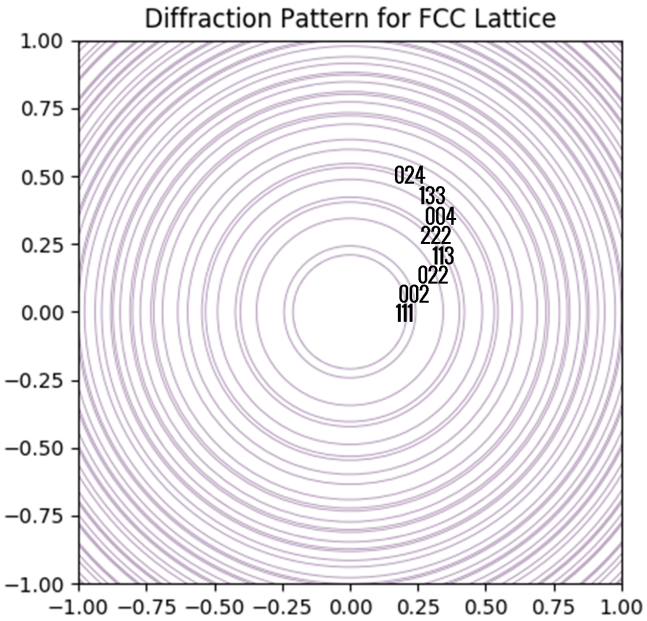

Figure 2: Theoretical pattern for the FCC lattice.

Note that only the relative sizes of the rings are relevant in the theoretical diffraction pattern, the absolute sizes are arbitrary, since an arbitrary camera constant K was chosen for the plot. This is why the units for the x and y axes are not stated. By resizing the plot to fit the diffraction patterns measured experimentally, the Miller indices of the rings can be determined via the relative size of the diffraction rings.

3.2 Diffraction Patterns

The measured diffraction patterns with an overlay of the theoretical diffraction pattern (Figure 2) are given in Figure 3. The left picture shows the pattern for a silver sample, the one on the right was generated by aluminum. The relative sizes of the rings in the measured diffraction patterns seem to agree very well with the ones in the theoretical pattern. This provides strong evidence that the crystal lattice in the materials silver and aluminum is indeed FCC. An interesting feature of both patterns is that the line with Miller indices 004 with respect to the conventional axes (6^{th} when counted from the center) is not visible, while the combination of lines 133 and 024 is again visible as one thick line. There are multiple factors determining the relative intensities of the diffraction rings (paraphrased from [3]):
The first one is the multiplicity of the Bragg planes. Since there are for example 12 Bragg planes with the same distance $d_{022} = d_{02\bar{2}} = d_{0\bar{2}2} = ...$, while there are only 6 Bragg planes with $d_{002} = d_{00\bar{2}} = d_{020} = ...$, the line 022 should have twice the intensity of 002, regarding only the effect of multiplicity. Another factor might be the effect of preferred orientation, which occurs when the crystalline deposits on the sample holder are not randomly oriented in space, but show preferred directions. In this case the diffraction lines show intensities different from what one would expect by only considering the multiplicities of the Bragg planes. In addition, there are the effects of extinction and absorption. The former effect occurs when waves are reflected at the underside of very strongly reflecting planes with an additional phase factor of π. This leads to negative interference with the wave reflected without additional phase factor and thus to a weaker diffraction line. The latter effect is due to the fact that the penetration depth and thus the absorption of the electron waves in the sample material might depend on the incident angle. Since the different diffraction lines were created by electron waves having different incident angles, the effect of absorption varies the relative intensities.
The combined effect of these factors would have to be considered to explain the relative intensities of the rings in the diffraction patterns above. Readers interested in modeling the relative intensities of the diffraction rings should refer to [3].

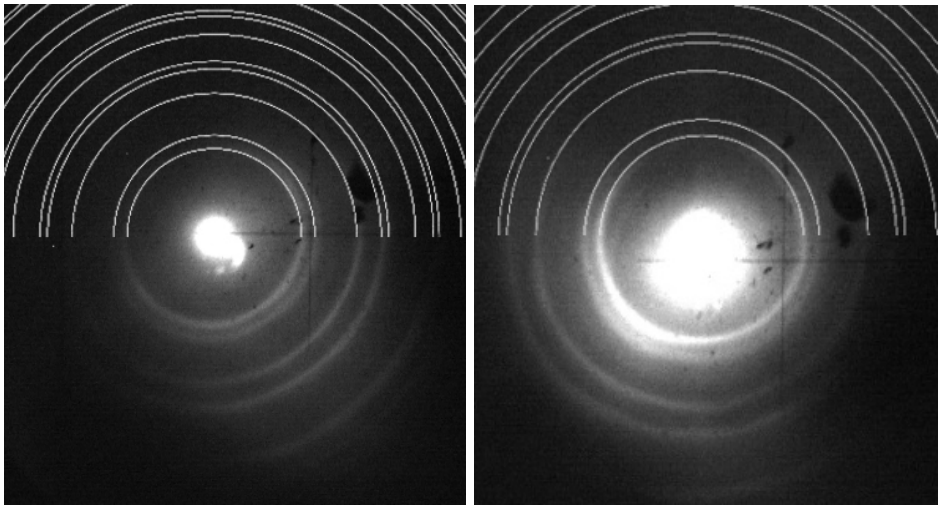

Figure 3: Diffraction patterns for silver (left) and aluminum (right) at 95 kV.

3.3 Camera Constant

The plot of the radius dependence of the camera constant K based on the silver sample (left in Figure 3) is given in Figure 4.

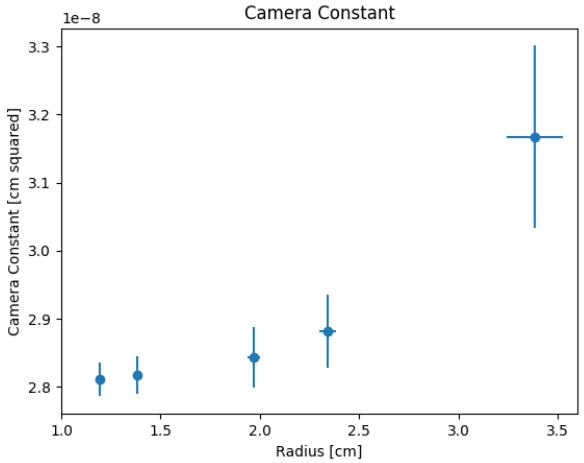

Figure 4: Plot of the camera constant K as a function of the radius D for the silver sample.

The camera constant varies between $2.8 \cdot 10^{-8}$ and $3.2 \cdot 10^{-8}$ cm^2 over a radius range from 1 to 3.5 cm. The values for K seem to increase as we go further away from the center of the diffraction pattern. This suggests that K is in fact not constant in D. However, since K only varies by approximately 15% from 1 to 3.5 cm, we still get a good agreement between the theoretical (based on a constant K) and the experimental (based on the actual K) patterns in Figure 3. The average over the values shown in the plot is (2.9 ± 0.1) cm^2. The uncertainties in the camera constant values increase with larger radii, since the larger rings are not completely visible in Figure 3, making the circle fitting in the software Traxis less precise. Especially the camera constant value for the largest ring should be treated with caution, as only a small portion of this ring is visible in Figure 3.

4 Conclusion

The theoretical diffraction pattern for the FCC lattice based on the theory of Fourier transformations matched well with the experimental patterns obtained in the TEM for the materials silver and aluminum. This verifies the theoretical predictions and shows that the atomic lattices of the two sample materials are indeed FCC. The analysis of the camera constant K showed that the assumption of its value being constant over the range of the diffraction rings is a good approximation, explaining the agreement of the experimental data with the theoretical pattern based on a constant K. The methods presented here can easily be adapted to other lattice types by starting with (1) and inserting the primitive reciprocal axis vectors of the lattice considered. Based on the resulting formula and using the methods presented above, theoretical patterns for other lattice types may then be plotted and compared to patterns obtained experimentally in TEM diffraction. This shows that TEM diffraction provides a powerful tool to analyze the atomic structure of many different crystalline materials.

References

[1] Advanced Undergraduate Laboratory: *TEM Electron Microscopy*, University of Toronto, https://www.physics.utoronto.ca/∼phy326/tem/tem.pdf, visited in Nov. 2017

[2] Kittel, Charles: *Introduction to Solid State Physics*. 8th edition, John Wiley and Sons Inc., 2005.

[3] James R. Connolly: *Introduction to X-Ray Powder Diffraction*. Spring 2012, http://epswww.unm.edu/media/pdf/06-Diffraction-II.pdf, visited in Nov. 2017

[4] National Physical Laboratory, UK: *What do 'high vacuum' and 'low vacuum' mean?*. http://www.npl.co.uk/reference/faqs/what-do-high-vacuum-and-low-vacuum-mean-(faq-pressure), visited in Nov. 2017